Comparative pathogenesis of two lineages of Powassan virus reveals distinct clinical outcome, neuropathology, and inflammation.

Erin S. Reynolds[1,2,3], Charles E. Hart[1,2,3, 4], Jacob T. Nelson[1,2,3,5], Brandon J. Marzullo[6,7], Allen T. Esterly[1,2,3, 8], Dakota N. Paine[1,2,3], Jessica Crooker[1,2,3], Paul T. Massa[1,9], Saravanan Thangamani[1,2,3#]

[1] Department of Microbiology and Immunology, SUNY Upstate Medical University, Syracuse, New York, USA

[2] SUNY Center for Vector-Borne Diseases, SUNY Upstate Medical University, Syracuse, New York, USA

[3] Institute for Global Health and Translational Science, SUNY Upstate Medical University, Syracuse, New York, USA

[4] Current address: Molecular Biology Section, Laboratory Sciences Directorate, Defense Centers for Public Health Aberdeen, Aberdeen Proving Grounds, MD, USA

[5] Current address: Lovelace Biomedical Research Institute, Albuquerque, New Mexico, USA

[6]Department of Biochemistry, Jacobs School of Medicine and Biomedical Sciences, SUNY Buffalo, Buffalo, New York, USA

[7] Genomics and Bioinformatics Core, New York State Center of Excellence Bioinformatics & Life Sciences, SUNY Buffalo, Buffalo, New York, USA

20 [8] Current address: Section of Infectious Diseases, Department of Internal Medicine, Yale School
21 of Medicine, New Haven, CT, USA

22 [9] Department of Neurology, SUNY Upstate Medical University, Syracuse, New York, USA

23 # Corresponding author

24 **Abstract**

25 Tick-borne flaviviruses (TBFV) can cause severe neuroinvasive disease which may result in death
26 or long-term neurological deficit in over 50% of survivors. Multiple mechanisms for invasion of
27 the central nervous system (CNS) by flaviviruses have been proposed including axonal
28 transport, transcytosis, endothelial infection, and Trojan horse routes. Flaviviruses may utilize
29 different or multiple mechanisms of neuroinvasion depending on the specific virus, infection
30 site, and host variability. In this work we have shown that infection of BALB/cJ mice with either
31 Powassan virus lineage I (Powassan virus) or lineage II (deer tick virus) results in distinct spatial
32 tropism of infection in the CNS which correlated with unique clinical presentation for each
33 lineage. Comparative transcriptomics of infected brains demonstrates activation of different
34 immune pathways and downstream host responses. Ultimately the comparative pathology and
35 transcriptomics are congruent with different clinical signs in a murine model. These results
36 suggest that different disease presentations would be occur in clinical cases due to the innate
37 differences in the two lineages of Powassan virus.

38

39

Author Summary

Powassan virus causes a nationally notifiable disease which can cause severe neurological disease in humans and has no approved vaccines or therapeutics. Although two distinct lineages circulate in North America, clinical differentiation is not typically performed, and pathology has been assumed to be similar between lineages. In this work, a direct comparison of lineage I (Powassan virus) and lineage II (deer tick virus) demonstrated distinct differences in the clinical presentation, pathology of the central nervous system, and immune response in immunocompetent mice. These differences suggest that deer tick virus and Powassan virus do not utilize the same mechanisms for neuroinvasion and dissemination within the CNS. This is clinically relevant as the development of treatment plans and therapeutics need to be evaluated for these virus lineages.

Introduction

Powassan virus is the only known TBFV circulating in North America and has two distinct genetic lineages. Prototypical Powassan virus, lineage I (POWV), was isolated in 1958 and known to be vectored by *Ixodes cookei* ticks [1,2]. Lineage II Powassan virus is also known as deer tick virus (DTV) and was initially isolated in 1995 and is vectored primarily by *Ixodes scapularis* ticks [3,4]. Powassan virus and DTV share approximately 84% nucleotide sequence identity and 94% amino acid identity but are serologically indistinguishable [5–8]. The number of cases and geographic range for both POWV and DTV have increased, coinciding with the expansion of *Ixodes* tick and increased surveillance. In addition, recent studies have demonstrated that

60 Powassan lineages may not only be vectored by *Ixodes* ticks but may also be transmitted by
61 some species of *Dermacentor*, *Amblyomma*, and *Haemaphysalis* ticks [9–11].

62 Infection with POWV is usually asymptomatic; however, some individuals will experience a
63 febrile illness that can progress to severe neuroinvasive disease that may present with
64 meningoencephalitis or paralysis. Case fatality rates are estimated to be between 10% to 15%,
65 and over 50% of POWV survivors experience long-term neurological sequelae [5,12]. While there
66 have been advances in the study of POWV neuroinvasive disease, the underlying pathology is
67 not completely defined, especially in relation to the similarly pathogenic DTV. Powassan virus
68 disease is a nationally notifiable condition but differentiation of lineages is not required [13].
69 When lineage differentiation is performed for human cases it is most often done through
70 sequencing of viral RNA as methods such as neutralization and immunohistochemistry use
71 antibodies which are cross reactive [14–17].

72 The neuropathology seen in POWV is currently believed to be mediated by a combination of
73 inflammatory cytokines breaching the integrity of the blood-brain barrier (BBB) and
74 intravasating leukocytes. Of possible relevance to differential POWV and DTV pathogenesis,
75 infections by clinically important TBFV may provide important clues on what determines
76 particular disease outcomes. For instance, the levels of TNFα, IL-1β, IL-6, and IL-8 have been
77 associated with the proinflammatory breakdown of the BBB through the loss of tight junctions,
78 with MMP-9 being crucial for neuroinvasive disease with tick-borne encephalitis virus (TBEV)
79 [18,19]. Once the integrity of the BBB has been compromised, the cellular destruction and
80 pathology associated with TBEV infection are driven by the migration of CD8+ T-lymphocytes
81 and NK cells [20]. Besides immune-mediated neuronal destruction, neuronal demise can occur

82 throughout the CNS with deficits related to the area in the brain damaged, as evidenced by
83 mapping a neuronal network with brains infected by the related Langat virus (LGTV) [21]. Noting
84 the differences in CNS pathogenesis of TBFV, we describe here essential differences in the
85 pathogenicity of POWV and DTV which are of relevance as historically they were assumed to be
86 interchangeable, which makes these findings novel and clinically relevant. As such, we propose
87 that the present studies support a reconsideration of distinct pathogenetic outcomes of
88 infection by POWV lineages in humans.

89 **Results**

90 **Immunocompetent mice inoculated with DTV and POWV had different clinical disease**
91 **presentations.**

92 We investigated whether equivalent doses of either DTV or POWV resulted in a different clinical
93 presentation in six-week-old BALB/cJ mice. The first outward signs of illness occurred at 5 days
94 post infection (dpi) when weight loss was observed in both infected groups (Fig. 1A, B).
95 Although weight loss occurred across both infected groups, it was more severe in the DTV-
96 infected mice. Seventy-five percent of DTV-infected mice (n=9) and 8% of POWV-infected mice
97 (n=1) reached loss of 20% or greater from their baseline weight and required humane
98 euthanasia (Fig. 1D). Starting at 6dpi generalized signs of febrile illness occurred in both groups
99 including ruffled coat, hunched posture, lethargy, and rapid or labored respiration. Ocular
100 discharge and closure of one or both eyes occurred in both infected groups between 6dpi and
101 8dpi but was more common in DTV-infected mice (50%, n=6) than POWV-infected mice (33%,
102 n=4.) Onset of neurological illness occurred at 6dpi in the POWV infected mice and at 7dpi for

103 the DTV infected mice and was markedly different between groups. Forty-two percent of DTV-
104 infected mice presented with neurological illness, including seizure (n=4) (Fig. 1D) and weak
105 grip which progressed to paralysis (n=1) (Fig. 1D). In contrast, neurological illness was present in
106 83% POWV-infected mice, with 25% mice exhibiting multiple signs. Observed signs in POWV-
107 infected mice included weak grip (n=3), paresis (n=3), loss of righting reflex/prostration (n=2),
108 seizure (n=1), and paralysis (n=5) (Fig. 1D).

109 Mean clinical disease scores and percent weight change from baseline were compared between
110 all groups until 8dpi, after which sample sizes were too small for statistical comparison.
111 Between 5dpi and 8dpi, there were statistically significant differences in the clinical disease
112 scores between uninfected mice and each infected group and between DTV and POWV infected
113 mice at the second daily observations on 6dpi [p=0.0404] and 7dpi [p=0.001] (Fig. 1A). Body
114 weight changes from baseline were significantly different between uninfected and each
115 infected group starting at 6dpi but not between DTV and POWV infected groups (Fig. 1B).

116 Differences in mean clinical disease scores and percent weight change from baseline were also
117 compared between male and female mice within a group. The DTV infected male and female
118 mice had significantly different clinical scores during the first daily observation at 7dpi
119 [p=0.0298] (Fig. S1A) and no significant differences were found in the POWV infected male and
120 female mice (Fig. S1F). In addition, trends in weight loss were consistent between male and
121 female DTV and POWV infected mice (Fig. S1B, G). Overall, DTV infected mice experienced a
122 higher degree of weight loss than POWV infected mice while POWV infected mice experienced
123 more loss of ambulation than DTV infected mice.

124 **Immunocompetent mice inoculated with DTV and POWV had the same time to death.**

125 Despite differences in clinical disease, all mice inoculated via footpad with 10^3 FFU of DTV or
126 POWV succumbed to disease between 6 and 11 dpi. Log-rank test (Mantel-Cox) did not show
127 significant differences in survival between DTV and POWV infected mice (Fig. 1C), which had
128 median survival times (MST) of 7.5 and 7 days, respectively. In addition, no significant
129 differences were present between male and female mice within a group (Fig. S1C, H) using the
130 same analyses. MST for DTV-infected mice were 7 days for males and 8.5 days for females,
131 while MST for POWV-infected mice were 7 days for both males and females.

132 **Viral titers differ in blood and tissues of DTV and POWV infected mice.**

133 Viral RNA was detected in blood samples from all DTV-infected mice and all except one POWV-
134 infected mouse between 1dpi and 3dpi (Fig. 1E). Viral RNA declined following 3dpi and was not
135 detected in blood samples after 9dpi. Mean viremia for the DTV group peaked on 2dpi at 1.798
136 Log FFU/µg RNA equivalents, while the POWV group peaked on 1dpi at 2.258 Log FFU/µg RNA
137 equivalents (Fig. 1E). At 1dpi, there was higher viremia in POWV-infected mice than in DTV-
138 infected mice [p=0.0314].

139 Detection of viral RNA in organs demonstrated that DTV and POWV disseminate throughout the
140 body. Viral RNA was present in the brain, popliteal lymph node from the injected leg, spleen,
141 and lung of all infected mice (Fig. 1F). There was viral RNA detected in the heart and kidney of
142 all DTV-infected mice and 92% POWV-infected mice (n=11.) Viral RNA was present at the
143 injection site for 50% of the mice in each infected group (n=6.) Limited viral RNA was found in

144 the liver with either no viral RNA or RNA below the detection limit in 92% DTV-infected mice
145 (n=11) and 67% POWV-infected mice (n=8.)

146 The highest amounts of viral RNA were detected in the brains of both infected groups, with an
147 average of 7.43 Log FFU/µg RNA equivalents present in the DTV group and 5.62 Log FFU/µg
148 RNA equivalents present in the POWV group (Fig. 1F). The brains of DTV-infected mice had
149 higher viral loads than POWV-infected mice [p=0.0096], while the POWV-infected mice had
150 higher viral loads in the lymph node [p=0.0002.] A comparison of viral RNA present in organs
151 was also performed between infected male and female mice and the only significant difference
152 was found in the livers of POWV-infected mice (Fig. S1I).

153 **Comparative Histopathology of Deer Tick Virus and Powassan Virus Infected Brains and Spinal**
154 **Cords.**

155 Histopathological changes were observed in POWV and DTV infected mouse brains across
156 multiple regions including the olfactory bulb (OB), cerebral cortex (CTX), hippocampal
157 formation (HPF), hypothalamus (HY), thalamus (TH), midbrain (MB), pons (P), medulla (MY),
158 and cerebellum (Purkinje layer: CB – P, granular layer: CB- G, molecular layer: CB – M) and
159 scored by severity (Table S2). Infected mice exhibited microgliosis and neuronal necrosis in the
160 cerebellum (Fig. 2A-C) and olfactory bulb (Fig. 2J-L), degenerating neurons and vacuolation of
161 neuropil were observed Ammon's horn of the hippocampal formation (Fig. 2D-F), and the
162 isocortex showed perivascular cuffing and meningoencephalitis (Fig. 2G-I). Deer tick virus
163 infected mice had higher lesion severity scores in the hippocampal formation, thalamus, and
164 midbrain regions compared to POWV infected mice (Fig. 3E,F).

165 Powassan virus infected brains showed meningoencephalitis (Fig. 2I) that had progressed into
166 the cervical spinal cord (Fig. 4C), while the meninges of the spinal cord appeared normal in DTV
167 infected samples (Fig. 4B). Cervical spinal cords of POWV infected mice exhibited considerable
168 histopathology in which nuclei of ventral gray matter motoneurons were either shrunken with
169 irregular cell bodies or had entirely degenerated (Fig. 4F). There was also conspicuous
170 extravasation of inflammatory cells in spinal cord gray matter of POWV infected mice,
171 especially in the cervical spinal cord (Fig. 4C, F, I, L). In contrast, neurons in the cerebellum and
172 spinal cord of DTV infected mice appeared normal in numbers and morphology (Fig. 2B, Fig. 4B,
173 E).
174 Brain sections stained for viral RNA and CD11b+ cells were examined and scored by severity in a
175 manner consistent with histopathological analysis (Table S3). Powassan virus and DTV infection
176 of neurons were noted throughout all infected animal brains; however, the regions infected
177 differed between viruses. The brains infected with POWV exhibited staining of viral RNA in all
178 regions but were concentrated primarily in the cerebellum and brainstem (Fig. 5C). Powassan
179 virus only rarely infected the hippocampus, isocortex, and olfactory bulb in most animals (Fig.
180 5G, H, K, L) compared to relatively high levels of infection of Purkinje cells and granule cells in in
181 the cerebellum (Fig. 5C).

182 Deer tick virus-infected brains showed a markedly different pattern of viral infection. There
183 was reduced infection in the cerebellum and brainstem (Fig. 5A, B) in comparison to POWV
184 infected brains but a pronounced increase of viral RNA found in neurons in the isocortex,
185 olfactory bulb, and hippocampal formation including the dentate gyrus granule cells and
186 pyramidal neurons in Ammon's horn (Fig. 5E, F, I, J). Virus severity scores show increased virus

187 in the cortex, hippocampal formation, and thalamus of DTV infected mice and increased virus in
188 the cerebellum of POWV infected mice (Fig. 3A, B). CD11b severity scores show an increased
189 positive cells in the hippocampal formation of DTV- compared to POWV- infected mice (Figure
190 3C).
191 Neuron specific staining differed in the spinal cords of POWV and DTV infected mice. In DTV
192 infected mice minimal viral RNA was present across the cervical, thoracic, and lumbar regions
193 (Fig. 6B, E, H, K). Prominent infection of cervical spinal cord neurons of POWV infected mice
194 was consistent with contiguous brainstem, cerebellum and midbrain regions that were also
195 positive for POWV. The presence of viral RNA-containing neurons decreased considerably from
196 cervical to thoracic and lumbar regions in several animals indicating that the cervical spinal cord
197 was particularly affected at this stage of infection (Fig. 6C, F, I, L). One POWV-infected mouse
198 had prominent infection of the hippocampus and isocortex (Table S3) however, this animal also
199 had the characteristic lower brain stem and spinal cord infection seen in the other POWV-
200 infected mice.

201 In summary, infection of the brainstem, cerebellum, and contiguous cervical spinal cord by
202 POWV correlates with the observed clinical signs seen during POWV infection, in which animals
203 exhibited substantial paralysis and motor deficits while infection with DTV was concentrated
204 mainly to the cerebral cortex, olfactory bulbs, and midbrain with less lower brainstem and
205 spinal cord involvement. The distinct regional patterns of infection by DTV and POWV are
206 depicted schematically in Figure 3B.

207 **Comparative Transcriptomics of POWV and DTV**

208 Transcripts from either DTV or POWV-infected brains were generated and compared against
209 the uninfected controls and represented increased levels of inflammatory cytokine and
210 chemokine genes (Fig. S3A, B; Fig. S4). The smallest p-adjusted value for either group was
211 STAT1, with genes involved in immunological signaling, inflammation, and interferon response
212 following infection (Fig. S3C, D). The 25 genes with the smallest p-values in POWV-infected
213 brains are involved with interferon signaling, antigen presentation and viral response (Fig. S6 C,
214 D). There was a significant upregulation in genes responsible for controlling viral infection in
215 both samples, including interferon-stimulated genes and innate immune signaling genes
216 associated with MyD88 and RIG-I like receptors. Individually, both POWV and DTV appear to
217 activate the JAK-STAT pathway through TLR stimulation and interferon production producing an
218 anti-viral state.

219 The transcript libraries generated from POWV- and DTV-infected brains were then compared
220 (Fig. 7A) and smaller libraries were generated based on GO enrichment analysis terms:
221 inflammatory response (Fig. 7B), immune system process (Fig. 7C), and defense response (Fig.
222 7D). The brain tissues infected with POWV had significantly higher levels of inflammatory
223 pathway genes including NLRP6 and chemokines associated with hematopoietic inflammatory
224 cell recruitment including CX3CR1. The tissues infected with DTV displayed higher levels of
225 Cav1, which induces NF-κB through T-cell activation. Furthermore, there is a strong difference
226 in the levels of CXCL3, with DTV-infected tissues having significantly higher levels of the
227 neutrophil chemotactic cytokine. The results from this comparison suggest that while there is a
228 similar pattern to the interferon response and establishment of the anti-viral state, DTV and

229 POWV infections of the CNS involve the recruitment of different cell types and activation of
230 different inflammatory pathways.

231 **Cytokine and chemokine analysis of terminal serum.**

232 Levels of 23 analytes were measured in terminal blood serum and evaluated to determine
233 differences between uninfected (n=12), DTV infected (n=11), and POWV infected (n=8) mice
234 (Fig. 8, Fig. S2). There were significantly higher levels of six analytes in DTV-infected groups
235 compared to uninfected groups: IL-10 [p=0.0321](Fig. 8D), IL-12(p40) [p=0.006](Fig. 8E), MCP-1
236 [p=0.031](Fig. 8G), MIP-1α [p=0.0059](Fig. 8H), MIP-1β [p=0.0237](Fig. 8I), and RANTES
237 [p=<0.0001](Fig. 8J). In contrast, there were only significantly lower levels in four analytes in
238 POWV-infected animals compared to controls: GM-CSF [p=0.0112](Fig. 8A), IL-2 [p=0.0249](Fig.
239 8B), IL-5 [p=0.0121](Fig. 8C), and IL-13 [p=0.0004](Fig. 8F). The only difference between DTV
240 and POWV was in IL-13 [p=0.0451](Fig. 8F). These data indicate an entirely different
241 proinflammatory response in the periphery following infection by these two viruses. Analytes
242 with no significant differences are shown in Fig. S2.

243 **Discussion**

244 Flaviviruses are endemic across much of the globe and cause millions of cases of human illness
245 each year [22]. Severity of neurotropic flaviviruses such as West Nile virus (WNV), Japanese
246 encephalitis virus (JEV), TBEV, and Powassan virus can range from mild to fatal and can cause
247 severe neuroinvasive disease with long-term sequelae in a high percentage of survivors. For
248 example, disease severity, fatality rate, and long-term sequelae associated with TBEV infection
249 has been shown to vary depending on the subtype despite the high sequence similarity

250 between these viruses [23,24]. Similarly, DTV and POWV share approximately 94% amino acid
251 identity and 84% nucleotide sequence similarity and are serologically indistinguishable [6–8].
252 Coupled with the lack of a vaccine or approved treatment and overlapping circulation in the
253 United States, testing to differentiate lineages is typically not performed for human cases.

254 **Immunocompetent mice inoculated with Powassan virus and Deer tick virus have different**
255 **clinical disease presentations.**

256 In this report, we have shown that DTV and POWV do not have the same clinical presentation
257 when inoculated via the same route and dosage. Common clinical signs in both virus groups
258 included ruffled fur, hunched posture, ocular discharge, and weight loss. The degree of weight
259 loss experienced by DTV-infected mice was more severe than POWV-infected mice. Seizure was
260 the most common neurological symptom present in DTV-infected mice and was consistent with
261 prominent infection and inflammation in the hippocampus. Mice infected with POWV
262 experienced neurological signs more consistent with infection and inflammation of the lower
263 brainstem, cerebellum and spinal cord including paresis and paralysis.

264 **Powassan virus and Deer tick virus induce neuronal death in differing regions of the brain**

265 The reduced levels of $CD11b^+$ cells seen in the histopathology of POWV-infected brains as
266 compared to the DTV-infected brains are congruent with the histopathology and spatial
267 distribution of the virus. The spatial distribution of POWV in the brain is concentrated in the
268 lower brain and spinal cord, while DTV preferentially infected and induced inflammation in the
269 hippocampus and isocortices, which suggests a different neuroinvasive route and/or spread of
270 infection in the brain. The neurologic clinical signs exhibited during late-stage infections are

271 dissimilar as well with DTV eliciting seizures while POWV neuropathology is manifested as
272 motor deficits. The comparative neuropathology of POWV and DTV reveals a stark contrast
273 which is recapitulated in chemokines, histopathology, and observed clinical signs; DTV infects
274 the hippocampus and isocortex, while POWV infection is concentrated within the cerebellum,
275 brain stem, and spinal cord. Interestingly, acute seizures have been linked to loss of the
276 pyramidal cell layer and neuronal loss in the hippocampus in Theiler's murine
277 encephalomyelitis virus-infected mice, which is consistent with pathology findings for mice that
278 experienced seizures in DTV-infected mice in the present work [25,26]. Published human cases of
279 fatal DTV infection have shown severe inflammation and infection of the cerebellum and
280 brainstem which is more consistent with neuropathology present in POWV-infected mice [14,15].
281 In these human cases limb weakness and difficulty ambulating were noted and are consistent
282 with the deficits we observed with mice with heavy infection in the cerebellum, brainstem, and
283 cervical spinal cord.

284 Changes in the clinical presentation of disease and pattern of infection in the CNS could be
285 attributed to a variety of factors, including person-to-person variability, site of infection, and
286 genomic diversity of viruses. Other flaviviruses have demonstrated that genetic diversity in the
287 E and NS5 regions change the phenotype of the virus including immunogenicity and
288 pathogenicity [27]. The strain of POWV or DTV used for inoculation, route and method of
289 inoculation and time spent replicating in the periphery could affect the clinical signs and
290 response to infection [21,23,28–30]. This is underscored by our findings in that the vectored route of
291 inoculation can cause a diverse set of clinical signs but ultimately be relegated to either a

292 cortical region meningoencephalitis or involve the cerebellum and spinal cord, resulting in
293 descending myelitis.

294 **Host Chemokine and Inflammatory Response to Powassan virus is different compared to Deer**
295 **tick virus.**

296 Neuroinvasion of flaviviruses has been shown to be a result of inflammatory breakdown of the
297 blood-brain barrier; however, other mechanisms may result in CNS infection as well. Our
298 findings are consistent with previous studies showing an upregulation of STAT1 and genes
299 associated with inflammation and interferon in the brain of moribund animals. The
300 histopathological differences seen between the regions of the brain infected by DTV and POWV
301 suggest a spatial tropism which may be affected by a region-specific neuroinvasion and
302 dissemination. The olfactory bulb of DTV-infected animals had high levels of virus present
303 which suggests that this area was significant for viral replication and consequent spreading to
304 cerebral cortex and to the underlying midbrain structures. The clinical signs in POWV-infected
305 animals combined with the histopathology clearly show myelitis and destruction of neurons in
306 the ventral horns of the cervical spinal cord, contiguous lower brain stem, and cerebellum,
307 illustrating a differing spatial tropism compared to DTV. The differences in these spatial
308 tropisms could be explained by differential routes of neuroinvasion, with DTV for instance
309 preferentially crossing the cribiform plate from olfactory neurons to infect the olfactory bulb,
310 while POWV may utilize retrograde axonal transport of virus from the periphery into the spinal
311 cord by the neural route or perhaps by a unique viremic route initiated by preferential
312 inflammatory degradation of the BBB in the spinal cord.

313 The comparative RNA-seq data suggests that there are different innate immune pathways
314 responding to DTV and POWV during CNS infection. While both viruses elicit a strong
315 interferon response, there is a significant increase in NLRP6 and IL1α transcripts in tissues
316 infected with POWV relative to tissues infected with DTV. There is also a significant increase in
317 CX3CR1 and AIRE genes which indicate the recruitment of CD8+ T-cells in POWV infected
318 tissues. The DTV-infected tissues conversely exhibit significant increases in CXCL3 CD177 and
319 CAV1, suggesting neutrophilic recruitment combined with T-cell dependent NF-κB transcription.
320 The spatial tropism exhibited in the histopathology is supported by the levels of Krt6a seen in
321 DTV-infected tissues, which exhibit anti-microbial properties in the olfactory bulb, an area with
322 extensive DTV infection. These findings suggest that the pathology seen in POWV is driven by
323 CD8+ cytotoxic T-lymphocytes, while DTV elicits repetitive NF-κB-mediated transcription and
324 inflammation. These findings are congruent with recent studies that suggest POWV is less
325 inflammatory in neuronal cell cultures and that the pathogenesis of POWV, like TBEV, is driven
326 by the extravasation of cytotoxic T-lymphocytes [20,31]. The response to POWV has recently been
327 expanded with experiments examining the role of TRIM5 in POWV infection [32]. We have also
328 noted in this report that TRIM5 is upregulated in both DTV and POWV infection compared to
329 uninfected controls; however, TRIM5 is also significantly upregulated in response to POWV as
330 contrasted to the response to DTV infection. This comparative view of RNA transcriptomics in
331 DTV and POWV infection illustrates a difference in cellular and inflammatory response to
332 infection.

333 In conclusion, a direct comparison of POWV (lineage I) and DTV (lineage II) demonstrated
334 distinct differences in clinical presentation and neuro-immunopathology. These differences

335 suggest these two viral lineages do not utilize the same routes of neuroinvasion and stimulate
336 distinct neuroimmunological responses.

337 **Methods**

338 **Ethics Statement**

339 Mouse experiments were conducted in an American Association for the Accreditation of
340 Laboratory Animal Care (AAALAC) approved facility within Animal Biosafety Level 3 (ABSL3)
341 containment. All procedures were performed in accordance with SUNY Upstate Medical
342 University Institutional Animal Care and Use Committee approved protocol (#455) which
343 adhered to the Guide for the Care and Use of Laboratory Animals [33].

344 **Viruses, animals, and infection**

345 Deer tick virus (Spooner strain) and POWV (LB strain) stocks were provided by the World
346 Reference Center for Emerging Viruses and Arboviruses at University of Texas Medical Branch
347 and had been previously passaged once in suckling mouse brains. Stocks were then passaged
348 six times on Vero E6 cells. Vero E6 cells (CRL-1586; American Type Culture Collection) were
349 cultured using Modified Eagle's Medium (MEM; Corning) and supplemented with fetal bovine
350 serum (FBS), non-essential amino acids, and penicillin/streptomycin antibiotic mixture and
351 maintained at 37°C with 5% CO_2. Virus titers were determined by focus-forming assay as
352 previously described [34].
353 Next generation sequencing demonstrated that the consensus nucleotide sequence of our DTV
354 stock was 99.84% identical to the DTV Spooner, Wisconsin isolate (GenBank: HM440560.1) and
355 our POWV stock was 99.96% identical to the POWV LB, Ontario isolate (GenBank:

356 NC_003687.1). Of 17 nucleotide differences between our DTV stock and DTV Spooner isolate
357 there were three resulting amino acid sequence differences in M (N213K), NS4B (S2368T), and
358 NS5 (K2903R). There were three nucleotide differences between our POWV stock and POWV LB
359 isolate resulting in one amino acid sequence difference in E (Q1436R) as well as one nucleotide
360 gap which may have resulted in one amino acid sequence difference in NS5 (W8255 to L or S).
361 Thirty-six 5-week-old male (n=18) and female (n=18) BALB/cJ mice were purchased from The
362 Jackson Laboratory (Bar Harbor, ME). Upon receipt, mice were housed three per cage in
363 individually ventilated cages with HEPA-filtered supply and exhaust air. Food and water were
364 provided *ad libitum*. Animals were provided a 12h light/12h dark cycle within a temperature
365 and humidity-controlled room. Mice were acclimated to the facilities for one week. On the day
366 of study initiation, prior to infection, animals were observed and weighed to ensure there were
367 no apparent physical abnormalities and that each group had a similar weight distribution.
368 Uninfected control mice had an average weight of 21.43g (± 2.09), DTV-infected mice had an
369 average weight of 20.74g (± 1.98), and POWV-infected mice had an average weight of 21.06g (±
370 2.16).

371 All mice received a single footpad injection of 30µL under isoflurane anesthesia. Control mice
372 received serum-free Dulbecco's Modified Eagle Medium (DMEM, Corning), and infected mice
373 received 10^3 focus forming units (FFU) of either POWV Lineage I (POWV LB) or Lineage II (DTV
374 Spooner). Each group contained six male and six female mice. These numbers were selected to
375 provide the minimum number of animals required to determine statistical significance between
376 sexes within a treatment group. Bodyweight measurements and detailed clinical observations
377 were performed daily to assess the animal appearance, behavior, respiration, and neurological

378 signs of disease (Table S1). Submandibular blood collection was performed from Days 0 to 7
379 using alternating cohorts of mice and alternating sites. Terminal blood was collected via cardiac
380 puncture following euthanasia.

381 When animals reached the criteria for humane euthanasia or at 11 days post-infection (dpi)
382 euthanasia was performed by CO_2 inhalation followed by cervical dislocation. Whole body
383 perfusion was performed using 10mL of sterile 0.9% sodium chloride, USP. Tissues collected at
384 necropsy were stored in either Buffer RLT (Qiagen) or 10% Neutral Buffered Formalin (NBF).
385 Blood was stored in Buffer RLT. Samples stored in Buffer RLT were maintained in ABSL3 facilities
386 for a minimum of 24 hours to allow inactivation. Samples stored in 10% NBF were fixed for a
387 minimum of 72 hours, with one change of NBF occurring 24 hours after collection.

388 No specific methods were used to minimize confounders or blind staff to group allocation
389 during the experiment. Each day procedures were performed with uninfected animals handled
390 first, followed by DTV-infected animals, and POWV-infected animals handled last. Equipment
391 and PPE were cleaned or changed between infected groups to prevent cross-contamination.

392 **Viral RNA detection via RT-qPCR**

393 Total RNA was extracted from blood and tissue samples using RNeasy Mini Kits (Qiagen) using
394 previously established modifications to the kit protocol [35]. RNA was quantified using a DS-11+
395 Spectrophotometer (Denovix) and tested for the presence of viral RNA by RT-qPCR on a Bio-Rad
396 CFX96 Touch Real-Time PCR System. Viral RNA was detected with forward
397 (CCGAGCCARRGTGAGGATGT), reverse (TCTTTTGCYGARCTCCACTT), and probe
398 (TTCATAGCGAAGGTKAGRTCCAACG) primers which have been previously validated to detect a

399 region of the NS5 gene conserved between POWV and DTV [36]. Standard curves for POWV and
400 DTV were generated from 10-fold dilutions of a known quantity of viral RNA and used to
401 estimate viral burden in experimental samples.

402 **Histology and RNA in situ hybridization**

403 Inactivated tissues from three male and three female mice per group were transferred to 70%
404 ethanol and shipped to Histowiz, Inc. for embedding and sectioning. Brains were sectioned at
405 5µM thickness and mounted on glass slides. Hematoxylin and eosin staining was performed at
406 Histowiz, Inc in accordance with their established methods. RNA in situ hybridization was
407 performed using RNAscope 2.5 HD Duplex kits (catalog 322430, Advanced Cell Diagnostics) per
408 manufacturer recommendations. Brain sections underwent dual staining protocol for POWV
409 positive-sense RNA probe (catalog 415641, Advanced Cell Diagnostics) and *Mus musculus*
410 integrin alpha M/CD11b (catalog 311491, Advanced Cell Diagnostics) to identify infected cells
411 and innate leukocytes. Spine sections underwent dual staining protocol using the same viral
412 RNA probe used on brain sections and *Mus musculus* RNA binding protein, fox-1 homolog (*C.*
413 *elegans*) 3/NeuN (catalog 481707, Advanced Cell Diagnostics), to identify infected cells
414 including $NeuN^+$ neurons. All slides were counterstained with a 50% solution of Gill's
415 hematoxylin I. Positive control samples were processed using *Mus musculus* Duplex Ppib and
416 Polr2a (catalog 321651, Advanced Cell Diagnostics) for process verification. Both Hematoxylin
417 and eosin staining and RNA in situ hybridization was performed on all brains sectioned.

418 Sagittal brain sections were examined in a rostro-caudal direction, including the olfactory bulb,
419 cerebral cortex, hippocampus, thalamus, hypothalamus, midbrain, pons, medulla oblongata,

420 and Purkinje, granular, and molecular layers of the cerebellum. Microscopic lesions, including
421 microgliosis, perivascular cuffing, and neuronal degeneration were graded as: 0 (absence of
422 lesions); 1 (minimal); 2 (mild); 3 (marked.) The presence of meningitis, encephalitis, and
423 meningoencephalitis were noted as M, E, and ME, respectively. RNAscope stained cells were
424 graded a: 0 (absence of staining); 1 (very few to low); 2 (moderate); 3 (numerous). Areas that
425 were not present were noted as NP.

426 **RNA Sequencing and Bioinformatics**

427 RNA sequencing and bioinformatics was performed for the same three male and three female
428 mice per group which had H&E and RNA in situ hybridization performed. Total RNA was quality
429 checked using an Agilent Fragment Analyzer to assess RNA quality and Qubit Fluorescence
430 (Invitrogen) to measure concentration. RNA libraries (200ng total starting material) were
431 prepared following the Illumina RiboZero Total Stranded RNA library prep kit using the ribosomal
432 removal protocol. Following library preparation, concentration and quality control, final libraries
433 were pooled to 10nM and the concentration of the pool was determined using the QuantaBio
434 Universal qPCR reaction kit. After dilution and denaturing, the pooled library was loaded onto an
435 Illumina NovaSeq6000 (PE100) for sequencing at 250pM as final concentration.
436 Per-cycle base call (BCL) files generated by the Illumina NovaSeq were converted to per-read
437 FASTQ files using bcl2fastq version 2.20.0.422 using default parameters. The quality of the
438 sequencing was reviewed using FastQC version 0.11.6. Detection of potential contamination
439 was done using FastQ Screen version 0.14.1. Finally, FastQC and FastQ Screen quality reports
440 were summarized using MultiQC version 1.9.0.

441 Adapter trimming was not performed. Genomic alignments were performed using HISAT2
442 version 2.2.1 using default parameters. Ensembl reference GRCm38 was used for the reference
443 genome and gene annotation set. Sequence alignments were compressed and sorted into
444 binary alignment map (BAM) files using sam tools version 1.3. Counting of mapped reads for
445 genomic features was performed using Subread feature Counts version 2.0.0 using the
446 parameters -p -s 2 –g gene_name –t exon –Q 60 -B -C, the annotation file specified with –a was
447 the Ensembl GRCm38 reference provided by Illumina's iGenomes. Alignment and feature
448 assignment statistics were summarized using MultiQC.
449 Differentially expressed genes were detected using the Bioconductor package DESeq2 version
450 1.38.1. Significance was set to an adjusted p-value less than or equal to 0.05. DESeq2 tests were
451 run for differential expression using a negative binomial generalized linear models, dispersion
452 estimates, and logarithmic fold changes. DESeq2 calculated log2 fold changes and Wald test p-
453 values as well as performing independent filtering and adjusted for multiple testing using the
454 Benjamini-Hochberg procedure to control the false discovery rate (FDR).
455 Gene ontology analysis was performed using the GOSeq Bioconductor package version 1.50.0.
456 GOSeq performs Gene Ontology analysis while addressing biases present in RNA-seq data not
457 found using other techniques, namely that expected read counts for a transcript are based on
458 both, the gene level of expression, and the length of the transcript. While other tools are
459 commonly used for GO term analysis, they do not account for this effect leading to results that
460 are biased toward GO terms with longer transcripts. The Wallenius approximation used by
461 GOSeq approximate GO term enrichment and calculated p-values for each GO category being

462 overrepresented among genes that were differentially expressed. These p-values were
463 corrected for multiple testing using the Benjamini-Hochberg Procedure.

464 **Cytokine and chemokine analysis of terminal serum**

465 Terminal serum samples were tested in duplicate for cytokine and chemokine levels on a Bio-
466 plex 200 (Bio-Rad) using a Bio-plex Pro Mouse Cytokine 23-plex assay according to kit
467 instructions. Cytokines detected were IL-1α, IL-1β, IL-2, IL-3, IL-4, IL-5, IL-6, IL-9, IL-10, IL-12
468 (p40), IL-12 (p70), IL-13, IL-17A, eotaxin, G-CSF, GM-CSF, IFN-γ, KC, MCP-1 (MCAF), MIP-1α,
469 MIP-1β, RANTES, and TNF-α. Serum was diluted 1:4 in the kit supplied diluent, incubated with
470 cytokine-specific labeled beads and detected with biotinylated antibody and streptavidin-PE.

471 **Statistical analysis**

472 Statistical analysis was conducted with GraphPad Prism software version 9.4.1 (GraphPad.) No
473 data were excluded from the analysis.

474 1 McLean DM, Best JM, Mahalingam S, Chernesky MA, Wilson WE. Powassan Virus: Summer
475 Infection Cycle, 1964. *Can Med Assoc J* 1964; **91**: 1360–1362.

476 2 McLean DM, Donohue WL. Powassan Virus: Isolation of Virus from a Fatal Case of
477 Encephalitis. *Can Med Assoc J* 1959; **80**: 708–711.

478 3 Telford SR, Armstrong PM, Katavolos P *et al.* A new tick-borne encephalitis-like virus
479 infecting New England deer ticks, Ixodes dammini. *Emerg Infect Dis* 1997; **3**: 165–170.

480 4 Ebel GD, Campbell EN, Goethert HK, Spielman A, Telford SR. Enzootic transmission of deer
481 tick virus in New England and Wisconsin sites. *The American Journal of Tropical Medicine*
482 *and Hygiene* 2000; **63**: 36–42.

483 5 Hermance ME, Thangamani S. Powassan Virus: An Emerging Arbovirus of Public Health
484 Concern in North America. *Vector Borne Zoonotic Dis* 2017; **17**: 453–462.

485 6 Beasley DWC, Suderman MT, Holbrook MR, Barrett ADT. Nucleotide sequencing and
486 serological evidence that the recently recognized deer tick virus is a genotype of Powassan
487 virus. *Virus Research* 2001; **79**: 81–89.

488 7 Kuno G, Artsob H, Karabatsos N, Tsuchiya KR, Chang GJ. Genomic sequencing of deer tick
489 virus and phylogeny of powassan-related viruses of North America. *The American Journal of*
490 *Tropical Medicine and Hygiene* 2001; **65**: 671–676.

491 8 Vogels CBF, Brackney DE, Dupuis AP *et al.* Phylogeographic reconstruction of the
492 emergence and spread of Powassan virus in the northeastern United States. *Proceedings of*
493 *the National Academy of Sciences* 2023; **120**: e2218012120.

494 9 Hart C, Hassett E, Vogels CBF, Shapley D, Grubaugh ND, Thangamani S. Powassan Virus
495 Lineage I in Field-Collected Dermacentor variabilis Ticks, New York, USA - Volume 29,
496 Number 2—February 2023 - Emerging Infectious Diseases journal - CDC.
497 doi:10.3201/eid2902.220410.

498 10 Raney WR, Herslebs EJ, Langohr IM, Stone MC, Hermance ME. Horizontal and Vertical
499 Transmission of Powassan Virus by the Invasive Asian Longhorned Tick, Haemaphysalis
500 longicornis, Under Laboratory Conditions. *Front Cell Infect Microbiol* 2022; **12**: 923914.

501 11 Sharma R, Cozens DW, Armstrong PM, Brackney DE. Vector competence of human-biting
502 ticks Ixodes scapularis, Amblyomma americanum and Dermacentor variabilis for Powassan
503 virus. *Parasites Vectors* 2021; **14**: 466.

504 12 Ebel GD. Update on Powassan Virus: Emergence of a North American Tick-Borne Flavivirus.
505 *Annual Review of Entomology* 2010; **55**: 95–110.

506 13 Clinical Evaluation & Disease | Powassan | CDC.
507 2023.https://www.cdc.gov/powassan/clinicallabeval.html (accessed 10 May2023).

508 14 Tavakoli NP, Wang H, Dupuis M *et al.* Fatal Case of Deer Tick Virus Encephalitis. *N Engl J*
509 *Med* 2009; **360**: 2099–2107.

510 15 Normandin E, Solomon IH, Zamirpour S *et al.* Powassan Virus Neuropathology and Genomic
511 Diversity in Patients With Fatal Encephalitis. *Open Forum Infect Dis* 2020; **7**.
512 doi:10.1093/ofid/ofaa392.

513 16 Solomon IH, Spera KM, Ryan SL *et al.* Fatal Powassan Encephalitis (Deer Tick Virus, Lineage
514 II) in a Patient With Fever and Orchitis Receiving Rituximab. *JAMA Neurology* 2018; **75**: 746–
515 750.

516 17 Piantadosi A, Rubin DB, McQuillen DP *et al.* Emerging Cases of Powassan Virus Encephalitis
517 in New England: Clinical Presentation, Imaging, and Review of the Literature. *Clin Infect Dis*
518 2016; **62**: 707–713.

519 18 Fortova A, Hönig V, Salat J *et al.* Serum matrix metalloproteinase-9 (MMP-9) as a biomarker
520 in paediatric and adult tick-borne encephalitis patients. *Virus Research* 2023; **324**: 199020.

521 19 Palus M, Bílý T, Elsterová J *et al.* Infection and injury of human astrocytes by tick-borne
522 encephalitis virus. *Journal of General Virology* 2014; **95**: 2411–2426.

523 20 Růžek D, Salát J, Palus M *et al.* CD8+ T-cells mediate immunopathology in tick-borne
524 encephalitis. *Virology* 2009; **384**: 1–6.

525 21 Chotiwan N, Rosendal E, Willekens SMA *et al.* Type I interferon shapes brain distribution
526 and tropism of tick-borne flavivirus. *Nat Commun* 2023; **14**: 2007.

527 22 Pierson TC, Diamond MS. The continued threat of emerging flaviviruses. *Nat Microbiol*
528 2020; **5**: 796–812.

529 23 Tkachev SE, Babkin IV, Chicherina GS *et al.* Genetic diversity and geographical distribution of
530 the Siberian subtype of the tick-borne encephalitis virus. *Ticks and Tick-borne Diseases*
531 2020; **11**: 101327.

532 24 Lindqvist R, Upadhyay A, Överby AK. Tick-Borne Flaviviruses and the Type I Interferon
533 Response. *Viruses* 2018; **10**. doi:10.3390/v10070340.

534 25 Bröer S, Käufer C, Haist V *et al.* Brain inflammation, neurodegeneration and seizure
535 development following picornavirus infection markedly differ among virus and mouse
536 strains and substrains. *Experimental Neurology* 2016; **279**: 57–74.

537 26 Stewart K-AA, Wilcox KS, Fujinami RS, White HS. Development of Post-infection Epilepsy
538 Following Theiler Virus Infection of C57BL/6 Mice. *J Neuropathol Exp Neurol* 2010; **69**:
539 1210–1219.

540 27 Davis EH, Beck AS, Li L *et al.* Japanese encephalitis virus live attenuated vaccine strains
541 display altered immunogenicity, virulence and genetic diversity. *NPJ Vaccines* 2021; **6**: 112.

542 28 Luethy LN, Erickson AK, Jesudhasan PR, Ikizler M, Dermody TS, Pfeiffer JK. Comparison of
543 three neurotropic viruses reveals differences in viral dissemination to the central nervous
544 system. *Virology* 2016; **487**: 1–10.

545 29 de Vries L, Harding AT. Mechanisms of Neuroinvasion and Neuropathogenesis by Pathologic
546 Flaviviruses. *Viruses* 2023; **15**: 261.

547 30 Tigabu B, Juelich T, Holbrook MR. Comparative analysis of immune responses to Russian
548 spring-summer encephalitis and Omsk hemorrhagic fever viruses in mouse models. *Virology*
549 2010; **408**: 57–63.

550 31 Nelson J, Ochoa L, Villareal P *et al.* Powassan Virus Induces Structural Changes in Human
551 Neuronal Cells In Vitro and Murine Neurons In Vivo. *Pathogens* 2022; **11**: 1218.

552 32 Chiramel AI, Meyerson NR, McNally KL *et al.* TRIM5α Restricts Flavivirus Replication by
553 Targeting the Viral Protease for Proteasomal Degradation. *Cell Reports* 2019; **27**: 3269-
554 3283.e6.

555 33 National Research Council (US) Committee for the Update of the Guide for theCare and Use
556 of Laboratory Animals. *Guide for the Care and Use of Laboratory Animals*. 8th ed. National
557 Academies Press (US): Washington (DC),
558 2011http://www.ncbi.nlm.nih.gov/books/NBK54050/ (accessed 11 May2023).

559 34 Rossi SL, Nasar F, Cardosa J *et al.* Genetic and Phenotypic Characterization of Sylvatic
560 Dengue Virus Type 4 Strains. *Virology* 2012; **423**: 58–67.

561 35 Hermance ME, Hart CE, Esterly AT, Reynolds ES, Bhaskar JR, Thangamani S. Development of
562 a small animal model for deer tick virus pathogenesis mimicking human clinical outcome.
563 *PLoS Negl Trop Dis* 2020; **14**. doi:10.1371/journal.pntd.0008359.

564 36 Hart CE, Bhaskar JR, Reynolds E *et al.* Community engaged tick surveillance and tickMAP as
565 a public health tool to track the emergence of ticks and tick-borne diseases in New York.
566 *PLOS Global Public Health* 2022; **2**: e0000215.

567

568 **Fig. 1.** Clinical presentation of DTV and POWV infection. Mice (n = 12 per group) were
569 inoculated via the footpad with 10^3 FFU of media (blue), DTV (green), or POWV (purple) and
570 monitored for signs of disease for up to 11 dpi. (A) Clinical signs of disease were categorized
571 and scored by severity (Table S1). Significant differences in DTV and POWV mice clinical scores

572 occurred at the PM observations on 6dpi and 7dpi. (B) Percent weight change from pre-
573 infection. Comparisons on (A) and (B) were made using one-way ANOVA with Šídák multiple
574 comparisons test. Error bars indicate SEM. (C) Survival of mice across all treatments were
575 evaluated using the Mantel-Cox log-rank test and median survival times (MST) were calculated.
576 (D) Humane euthanasia was performed when mice met specific criteria and are categorized to
577 demonstrate differences between DTV and POWV with date of death shown above each bar. (E,
578 F) Blood was collected from alternating cohorts of male (n=3) and female (n=3) mice from 0 to
579 7dpi and at termination blood and tissues (brain, popliteal lymph node, heart, kidney, liver,
580 injection site, spleen, and lung) were collected from all animals to determine viral loads via rt-
581 qPCR. For brain analysis, six animals per group (3M and 3F) were tested and for all other tissues
582 twelve animals (6M and 6F) were tested. Viral loads are expressed as Log FFU equivalents per
583 microgram of RNA after normalization to a standard curve. Comparisons on (D) and (E) were
584 performed using two-tailed Student's t-test with Welch's correction.
585 **Fig. 2.** Neuropathological examination of DTV and POWV infected mouse brains. Uninfected
586 mouse with normal structures shown in (A) cerebellum with insets showing molecular cell layer
587 – M, Purkinje cell layer – P, and granular cell layers – G, (D) Ammon's horn of the hippocampus,
588 (G) isocortex, and (J) olfactory bulb. Cerebellum of DTV (B) and POWV (C) infected mice with
589 microgliosis (inset, red arrow) and neuronal cell necrosis (inset, black arrowheads). Ammon's
590 horn of the hippocampus from DTV (E) and POWV (F) infected mice with neuropil vacuolation
591 (inset, red arrow) and hyper eosinophilic degenerating neurons (inset, black arrow). Isocortex
592 of DTV (H) and POWV (I) with infiltration of leptomeninges (inset, black arrow) and perivascular

593 cuffing (inset, red arrow). Olfactory bulb of DTV (K) and POWV (L) infected mice with neuronal
594 cell necrosis in granular cell layers (black arrow).

595 **Fig. 3.** Severity of virus,CD11b, and lesions in DTV and POWV-infected mouse brains by region.
596 (A) Virus severity individual mice by region and (B) brain regions of DTV infected mice had
597 statistically more virus severity in CTX, HPF, and TH while POWV infected mice had more virus
598 severity in CB. (C) CD11b severity of individual mice by region. (D) Brain regions of DTV infected
599 mice had statistically significant increases in CD11b positive cells in HPF. (E) Severity of
600 individual mice by region. (F) Brain regions of DTV infected mice had statistically significant
601 differences in severity in the HPF, MB, and TH regions. All comparisons performed using
602 unpaired two-tailed Student's t-test with Welch's correction.

603 **Fig. 4.** Neuropathological examination of DTV and POWV infected mouse spinal cords.
604 Uninfected mouse with normal structures shown in (A, D) cervical region (black arrow shows
605 motor neuron in ventral horn), (G) thoracic region, and (J) lumbar region. DTV infected mouse
606 (B) cervical region, (E) motor neuron (black arrow) in dorsal horn, (H) thoracic region, and (K)
607 lumbar region. POWV infected mouse with (C) meningoencephalitis (red arrow) in cervical
608 region, (F) absent and degenerating motor neuron (black arrow) in dorsal horn, and infiltrations
609 in (I) thoracic and (L) lumbar regions.

610 **Fig. 5.** Divergent patterns of infection in DTV and POWV infected mouse brains. Representative
611 images of DTV infected (A, B, E, F, I, J) and POWV infected (C, D, G, H, K, L) brains stained for
612 viral RNA (teal) and $CD11b^{+}$ cells (pink). (A – D) Molecular (green M), Purkinje (green P), and
613 granular (green G) cell layers of the cerebellum and (C) POWV infected Purkinje cells (black
614 arrow). (E) CD11b positive cells (black arrow) around a vessel in the hippocampal region of a

615 DTV infected mouse brain. (H) Minimal infected cells (black arrow) in the hippocampal region of
616 a POWV infected mouse brain. (I) CD11b positive cells around a vessel (black arrow) and in the
617 leptomeninges (red arrow) of the isocortex of a DTV infected mouse brain. (K) CD11b positive
618 cells in the perivascular (Virchow-Robin) space (black arrow) of a POWV infected mouse brain.

619

620 **Fig. 6.** Divergent patterns of infection in DTV and POWV-infected mouse spinal cords.
621 Representative images of uninfected, DTV infected, and POWV infected mouse spinal cord with
622 teal staining of viral RNA and pink staining of neuronal nuclei (NeuN.) Uninfected cervical (A, D),
623 thoracic (G), and lumbar (J) regions with normal motor neurons shown (D, red arrows). DTV
624 infected mouse spinal cord cervical (B, E), thoracic (H), and lumbar (K) regions with minimal
625 infected neurons. POWV infected mouse spinal cord cervical (C, F), thoracic (I), and lumbar (L)
626 regions with decreasing infection across the cord and degenerating motor neurons (F, black
627 arrows.)
628 **Fig. 7.** RNA sequencing analysis of brain tissue. Brains were harvested at time of euthanasia and
629 stored in trizol before homogenization and RNA extraction followed by RNA-Seq. Transcript
630 libraries were analyzed using R with (A) POWV compared to DTV. Genes were separated into
631 smaller gene ontology sets and compared for (B) inflammatory response (C) immune system
632 process and (D) defense response.
633 **Fig. 8.** Cytokine and chemokine levels were measured in terminally collected serum from
634 uninfected (n = 6M/6F), DTV infected (n = 5M/6F), and POWV infected (n = 3M/5F) mice by Bio-
635 Plex Mouse Cytokine 23-plex panel. Significant differences were present between uninfected
636 and POWV-infected mice for four parameters (A, B, C, F), between uninfected and DTV-infected

637 mice for six parameters (D, E, G, H, I, J), and between DTV-and POWV infected mice for one
638 parameter (F). Comparisons were made using Brown-Forsythe and Welch's ANOVA test with
639 Dunnett's T3 multiple comparisons test.

640

641 **Fig. S1.** Comparison of differences between male and female mice infected with DTV or POWV.
642 Male (n = 6) and female (n = 6) DTV-infected mice had significantly different clinical observation
643 scores (A) on 7dpi at the AM observation [p = 0.0298] and changes to body weights (B) at 3dpi
644 [p = 0.04673]. No significant differences were found in survival (C), or viral RNA detected in
645 tissues (D) or blood (E). Male (n = 6) and female (n = 6) POWV-infected mice had significantly
646 different changes to body weights (G) at 4dpi [p = 0.03196] and differences in the amount of
647 viral RNA present in their livers (I) [p = 0.0257]. No significant differences were found in the
648 clinical observation scores (F), survival (H), or viral RNA present in the blood (J). Comparisons
649 were made using unpaired, two-tailed Student's t-test with Welch's correction. Error bars show
650 SEM.

651 **Fig. S2.** Cytokine and chemokine levels were measured in terminally collected serum from
652 uninfected (n = 6M/6F), DTV infected (n = 5M/6F), and POWV infected (n = 3M/5F) mice by Bio-
653 Plex Mouse Cytokine 23-plex panel. No significant differences were found between groups for
654 13 analytes. Comparisons were made using Brown-Forsythe and Welch's ANOVA test with
655 Dunnett's T3 multiple comparisons test.

656 **Fig. S3.** RNA sequencing analysis of brain tissue. Brains were harvested at moribundity and
657 stored in trizol before homogenization and RNA extraction followed by RNA-Seq. Transcript

658 libraries were analyzed using R with (A) POWV and (B) DTV compared to uninfected controls and
659 the 25 smallest adjusted p-values represented in a heat map for (C) POWV and (D) DTV.

660 **Fig. S4.** GO Term analysis of RNA sequencing from infected brain tissue. Transcripts from
661 previous RNA sequencing (Fig. 4, SI Appendix – Fig. S6) analyzed using Kyoto Encyclopedia of
662 Genes and Genomes (KEGG) using R for the top 25 overrepresented GO terms for (A) POWV and
663 (B) DTV compared to uninfected controls and (C) POWV compared to DTV.

664 **Table S1.** Clinical observation categories and scores. The highest scoring observation within a
665 category determined the score for the category. Scores from each category were added to
666 determine the total score.

667 **Table S2.** Distribution and severity of histologic lesions in brains. H&E-stained brain sections
668 were assessed for microscopic lesions including microgliosis (MG), perivascular cuffing (PC), and
669 neuronal necrosis (NN). Semi-quantitative scoring is indicated by 0 (absence of lesions), 1 (very
670 few to low), 2 (moderate), and 3 (numerous). Meningitis (M), encephalitis (E), and
671 meningoencephalitis (ME) were also noted. Areas that were not present were noted as NP.

672 **Table S3.** Presence of viral RNA and CD11b in the brain via RNAscope. Staining for viral RNA
673 (teal) and CD11b (pink) was performed using RNAscope. Brain regions were semi-quantitatively
674 scored with 0 (absence of staining), 1 (very few to low), 2 (moderate), and 3 (numerous).
675 Meningitis (M), encephalitis (E), and meningoencephalitis (ME) were also noted. Areas that
676 were not present were noted as NP.

677

678 **Table S4.** RNA-Seq full list of comparisons by gene for POWV vs DTV group.

679 **Table S5.** RNA-Seq full list of comparisons by gene for POWV vs Control group.

680 **Table S6.** RNA-seq full list of comparisons by gene for DTV vs Control group.

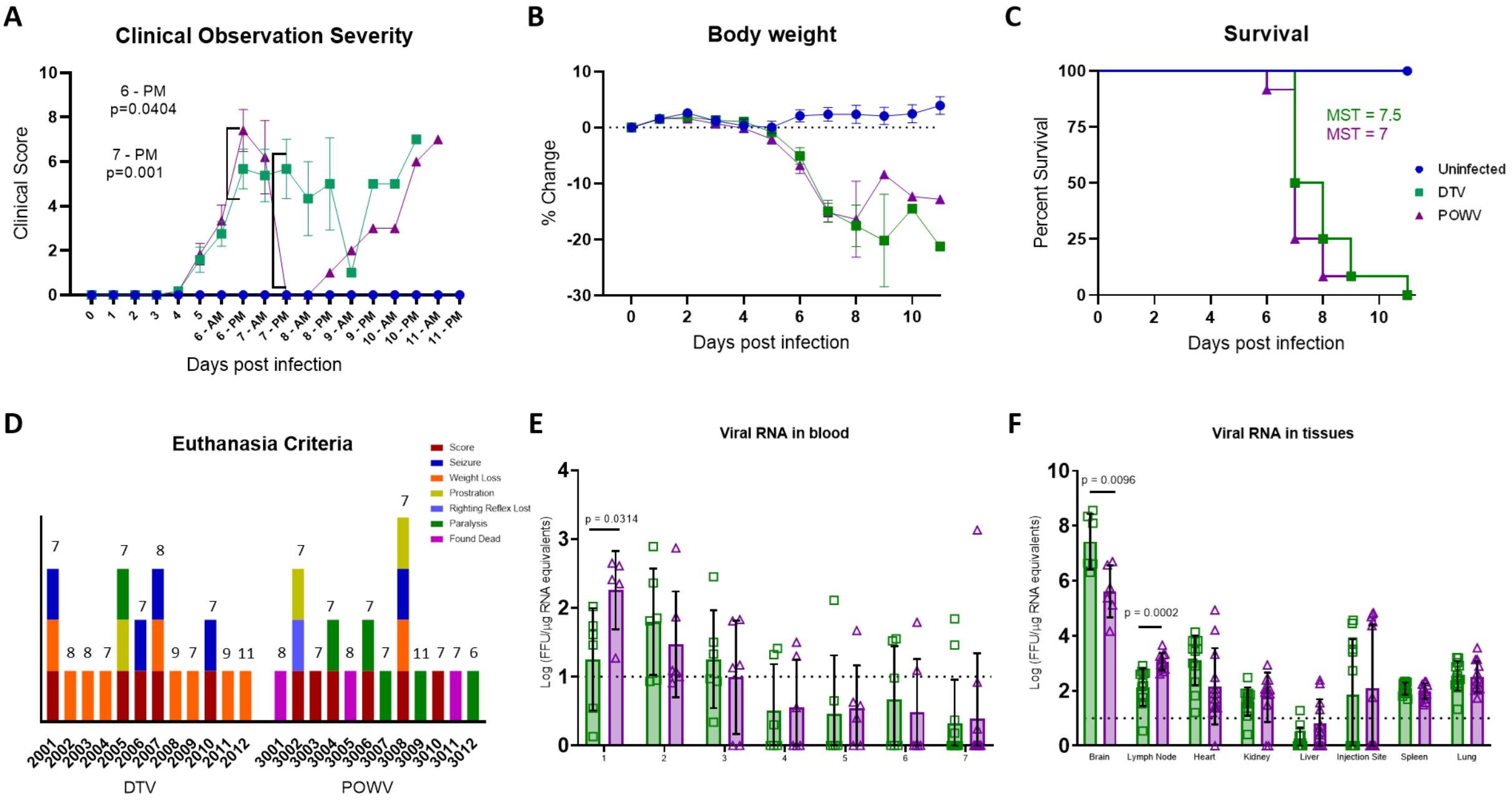
A
Clinical Observation Severity
Clinical Score
6 - PM
p=0.0404
7 - PM
p=0.001
Days post infection
B
Body weight
% Change
Days post infection
C
Survival
Percent Survival
MST = 7.5
MST = 7
Uninfected
DTV
POWV
Days post infection
D
Euthanasia Criteria
Score
Seizure
Weight Loss
Prostration
Righting Reflex Lost
Paralysis
Found Dead
DTV
POWV
E
Viral RNA in blood
Log (FFU/µg RNA equivalents)
p = 0.0314
F
Viral RNA in tissues
Log (FFU/µg RNA equivalents)
p = 0.0096
p = 0.0002
Brain
Lymph Node
Heart
Kidney
Liver
Injection Site
Spleen
Lung

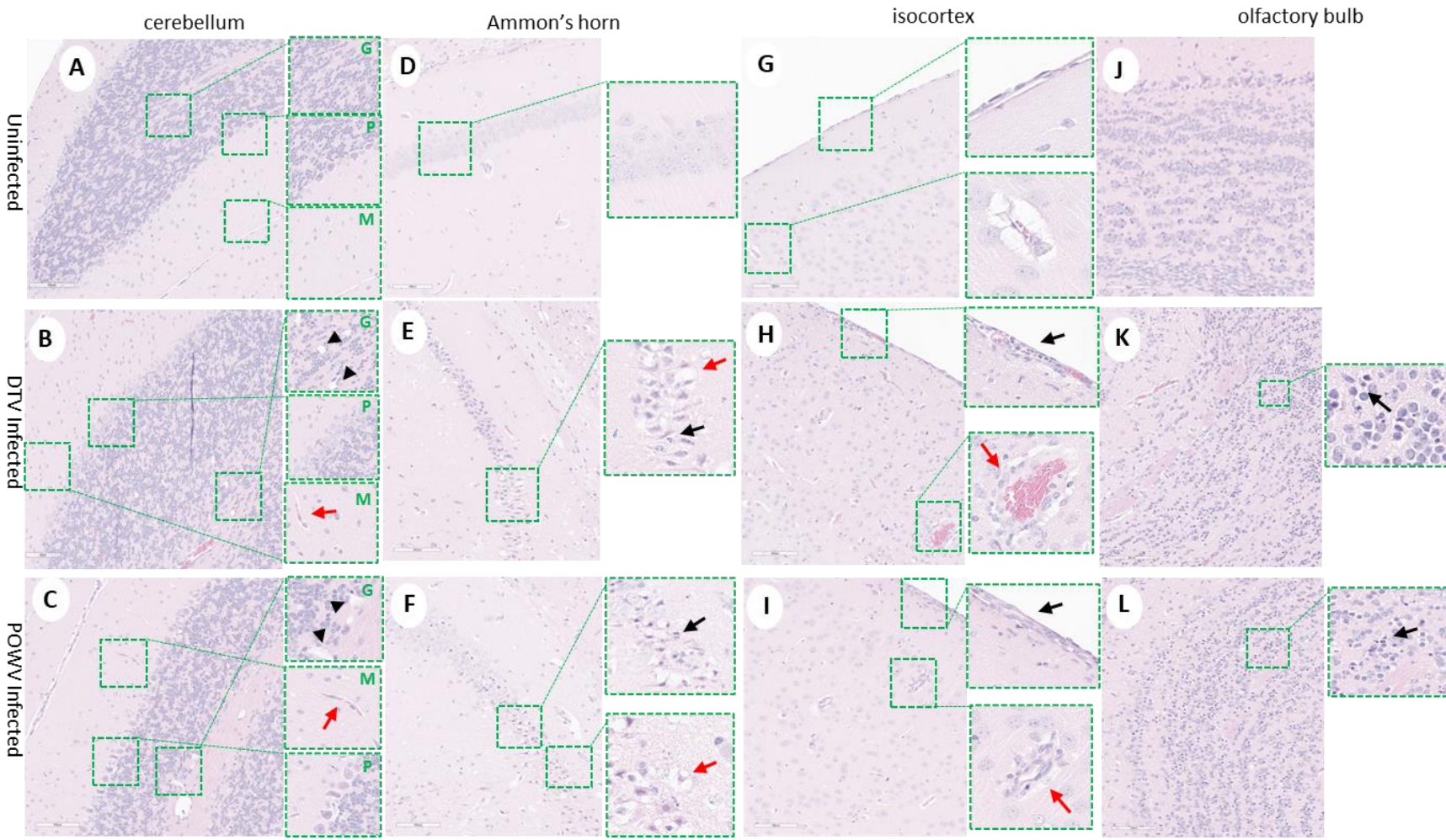
cerebellum
Ammon's horn
isocortex
olfactory bulb
Uninfected
DTV Infected
POWV Infected
A
B
C
D
E
F
G
H
I
J
K
L
G
P
M

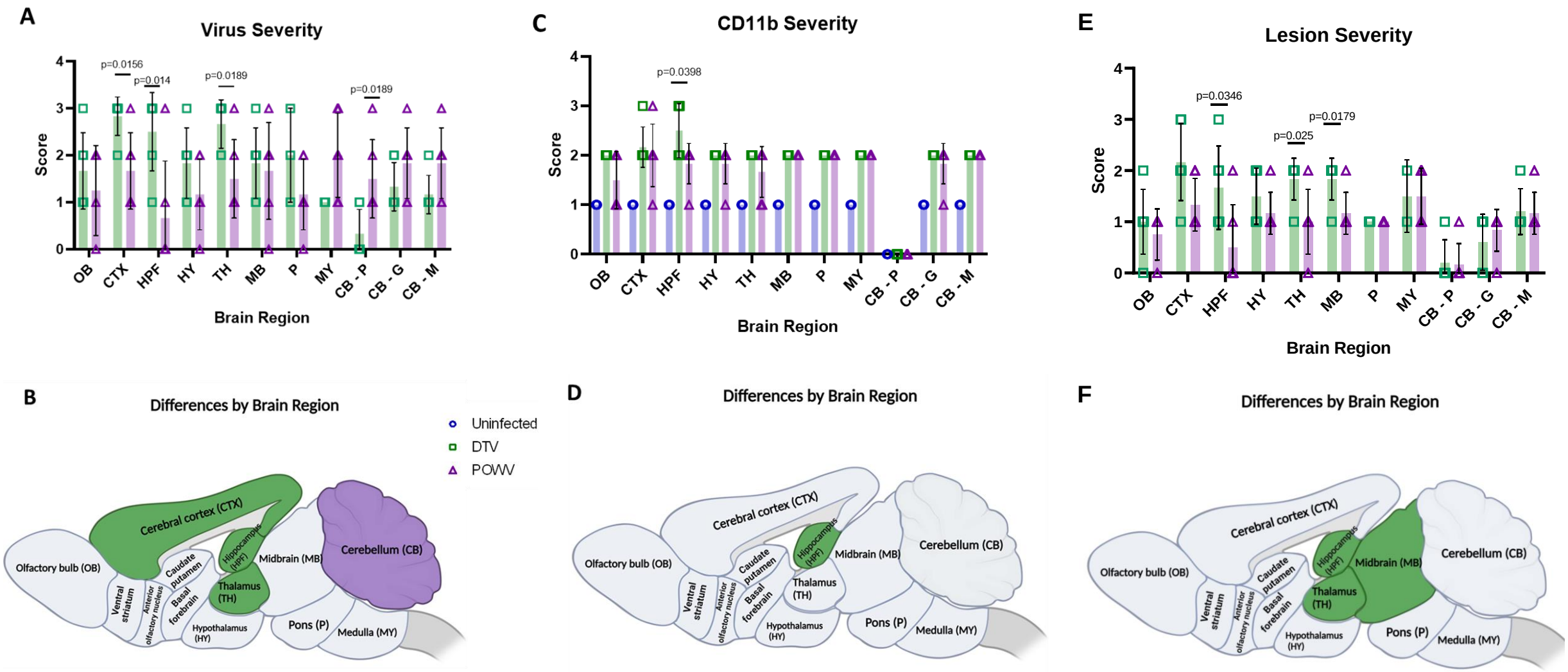
A
Virus Severity
Score
Brain Region
p=0.0156
p=0.014
p=0.0189
p=0.0189
OB
CTX
HPF
HY
TH
MB
P
MY
CB - P
CB - G
CB - M
C
CD11b Severity
p=0.0398
E
Lesion Severity
p=0.0346
p=0.025
p=0.0179
B
Differences by Brain Region
Uninfected
DTV
POWV
Cerebral cortex (CTX)
Olfactory bulb (OB)
Hippocampus (HPF)
Caudate putamen
Midbrain (MB)
Cerebellum (CB)
Ventral striatum
Anterior olfactory nucleus
Basal forebrain
Thalamus (TH)
Hypothalamus (HY)
Pons (P)
Medulla (MY)
D
F

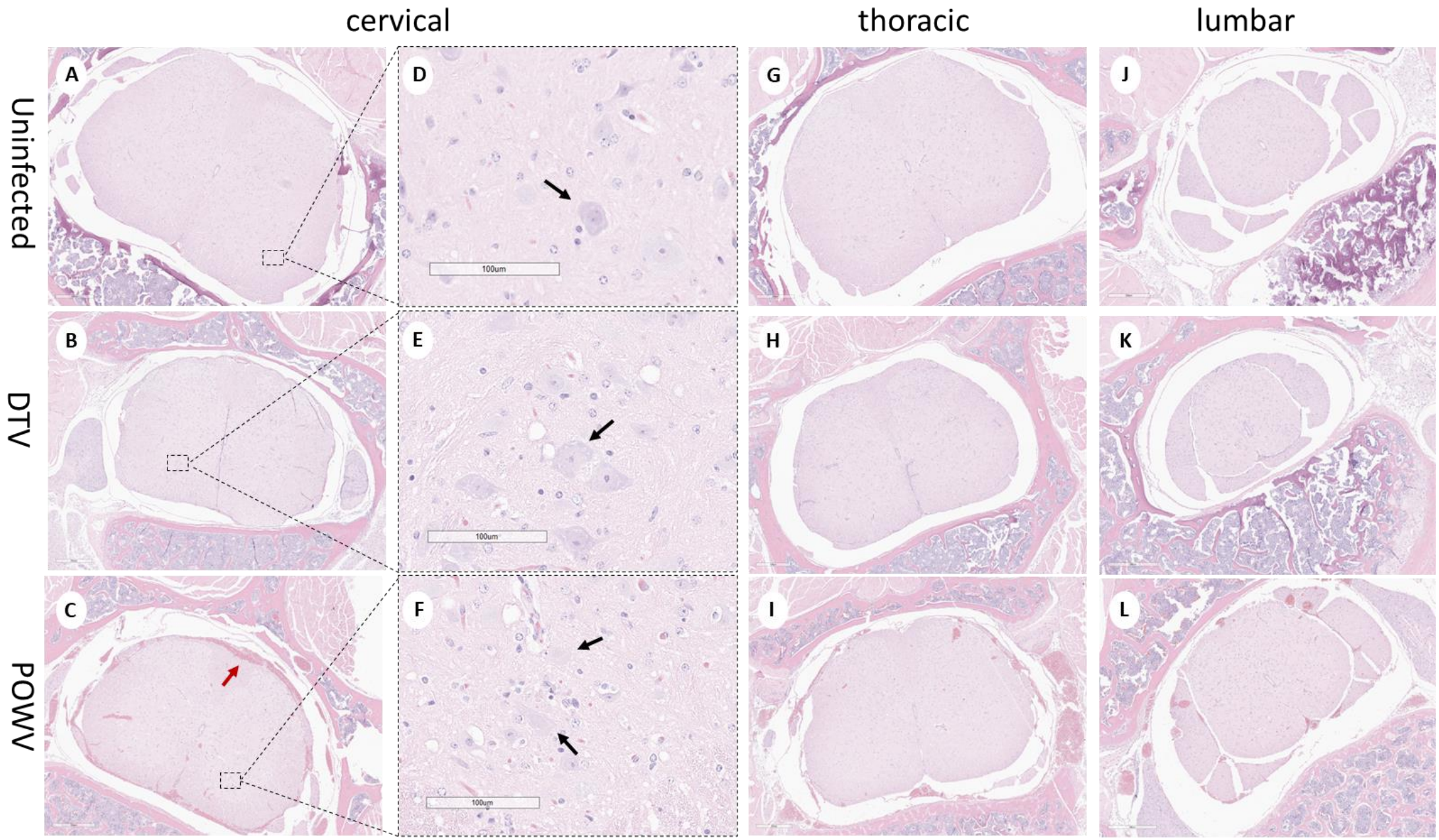
cervical
thoracic
lumbar
Uninfected
DTV
POWV
A
B
C
D
E
F
G
H
I
J
K
L
100um
100um
100um

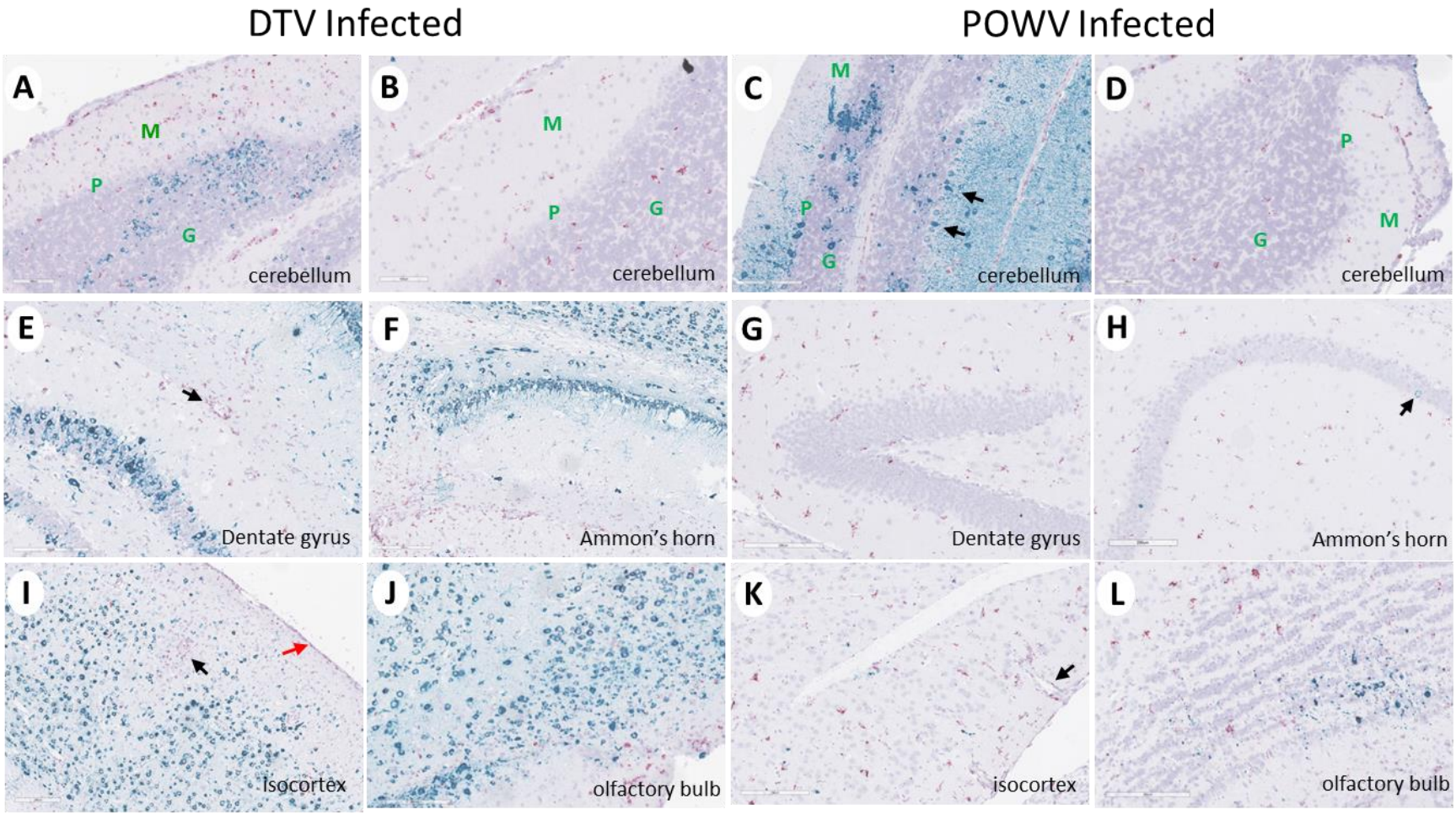
DTV Infected
POWV Infected
A
M
P
G
cerebellum
B
M
P
G
cerebellum
C
M
P
G
cerebellum
D
P
M
G
cerebellum
E
Dentate gyrus
F
Ammon's horn
G
Dentate gyrus
H
Ammon's horn
I
Isocortex
J
olfactory bulb
K
isocortex
L
olfactory bulb

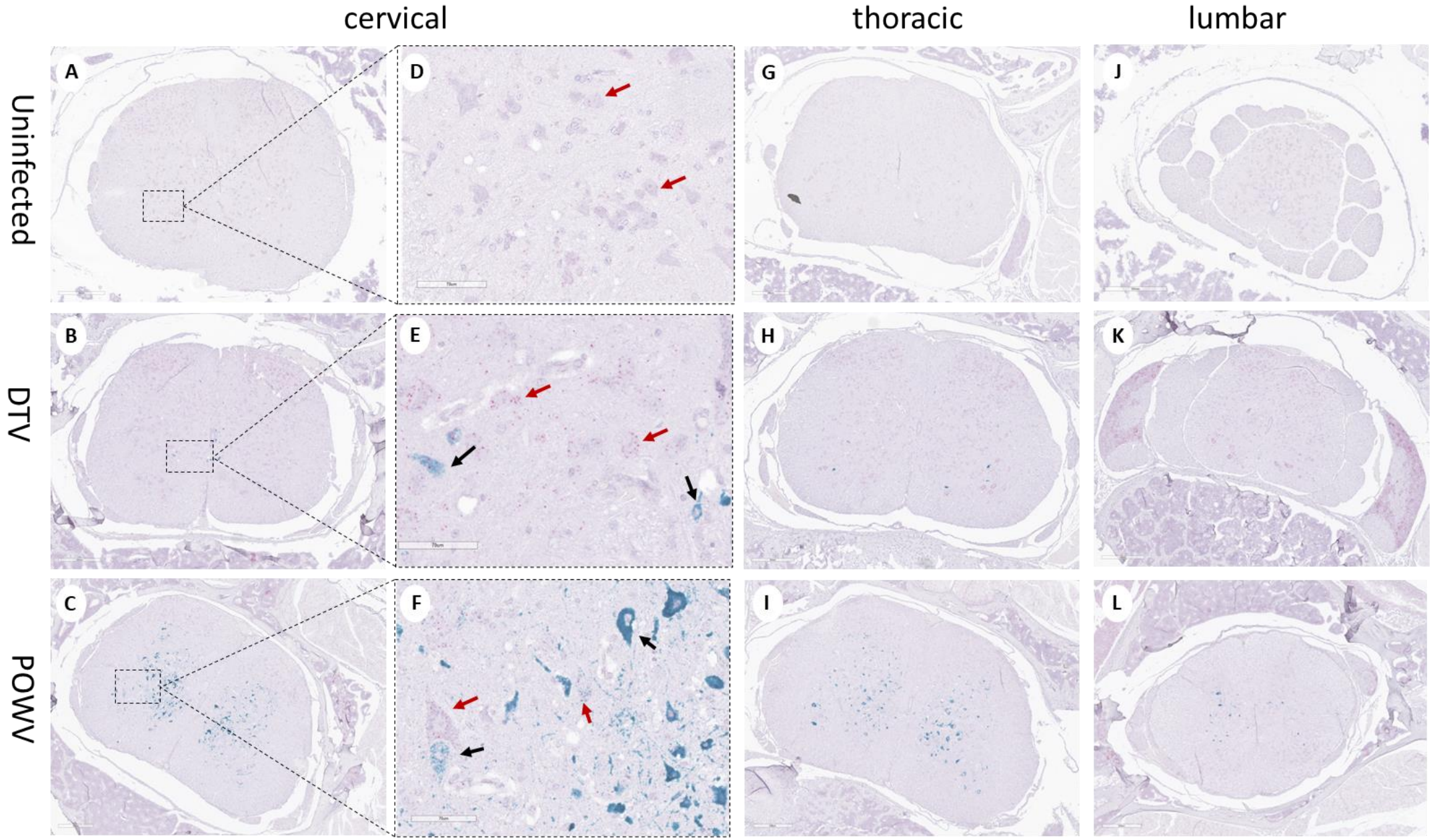
cervical
thoracic
lumbar
Uninfected
DTV
POWV
A
B
C
D
E
F
G
H
I
J
K
L

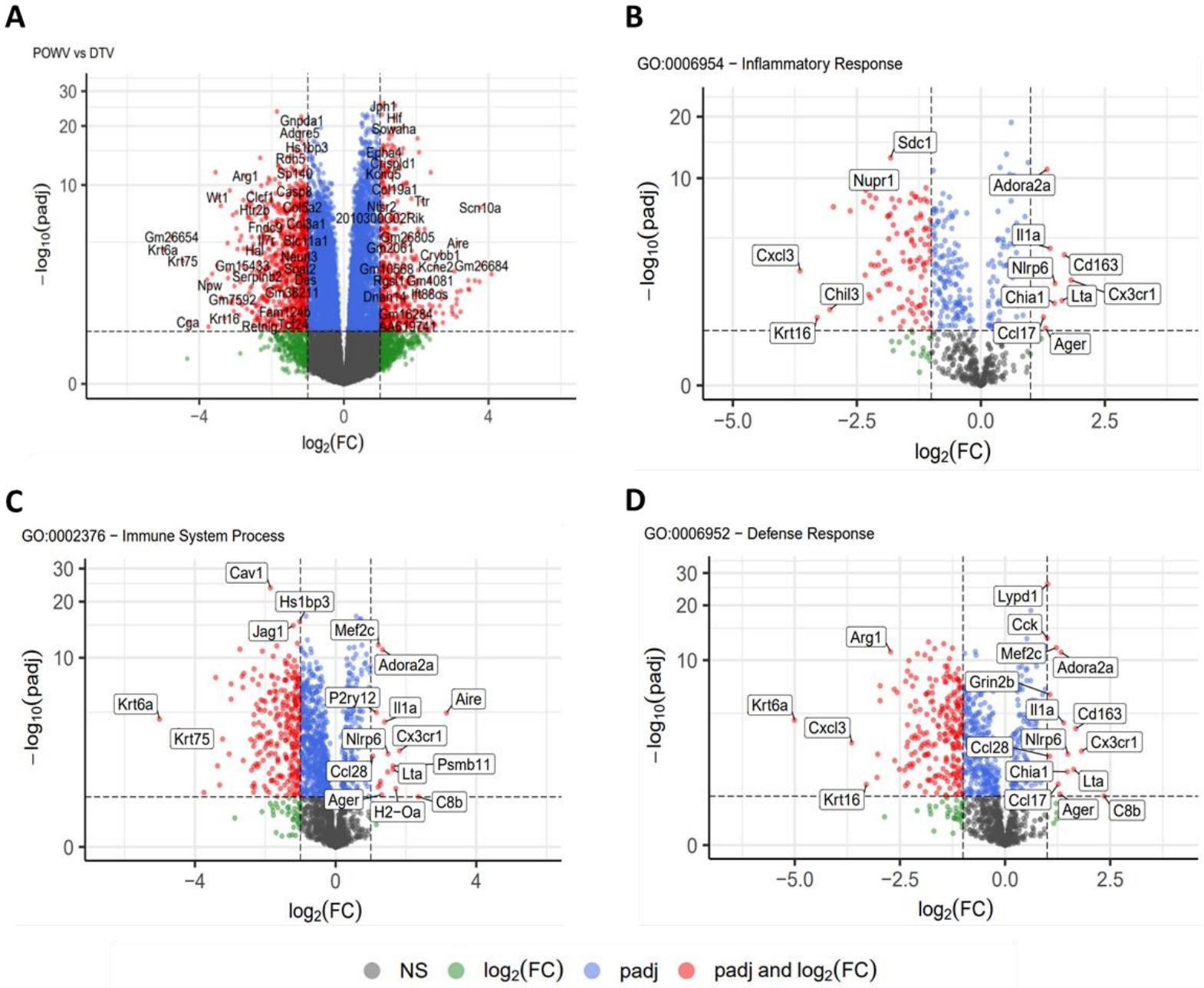
A
POWV vs DTV
−log10(padj)
log2(FC)
B
GO:0006954 − Inflammatory Response
Sdc1
Nupr1
Adora2a
Il1a
Cxcl3
Nlrp6
Cd163
Chil3
Chia1
Lta
Cx3cr1
Krt16
Ccl17
Ager
C
GO:0002376 − Immune System Process
Cav1
Hs1bp3
Jag1
Mef2c
Adora2a
Krt6a
P2ry12
Il1a
Aire
Krt75
Nlrp6
Cx3cr1
Ccl28
Lta
Psmb11
Ager
C8b
H2−Oa
D
GO:0006952 − Defense Response
Lypd1
Cck
Arg1
Mef2c
Adora2a
Grin2b
Krt6a
Il1a
Cd163
Cxcl3
Nlrp6
Cx3cr1
Ccl28
Chia1
Lta
Krt16
Ccl17
Ager
C8b
NS
log2(FC)
padj
padj and log2(FC)

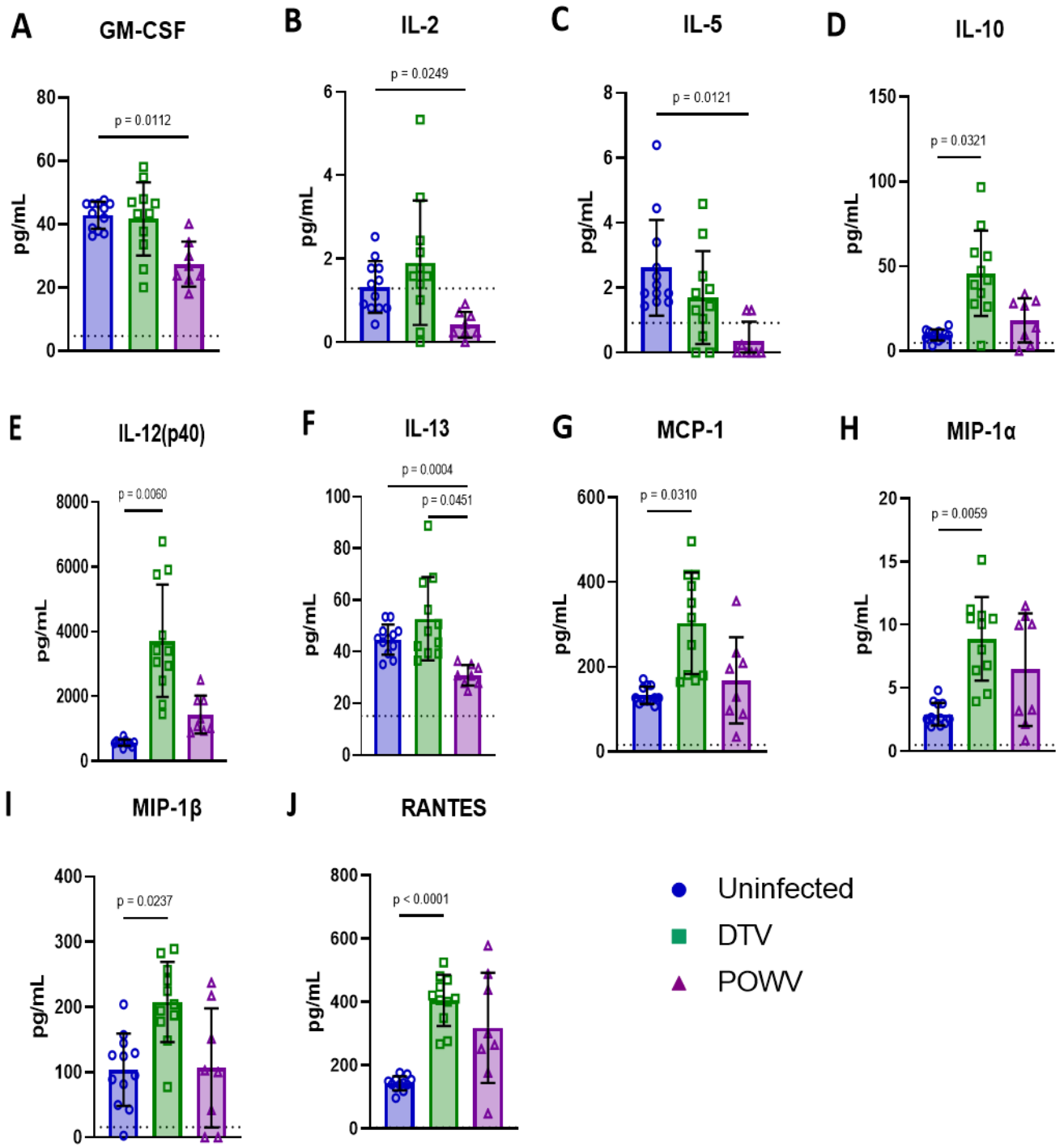
A
GM-CSF
p = 0.0112
pg/mL
B
IL-2
p = 0.0249
pg/mL
C
IL-5
p = 0.0121
pg/mL
D
IL-10
p = 0.0321
pg/mL
E
IL-12(p40)
p = 0.0060
pg/mL
F
IL-13
p = 0.0004
p = 0.0451
pg/mL
G
MCP-1
p = 0.0310
pg/mL
H
MIP-1α
p = 0.0059
pg/mL
I
MIP-1β
p = 0.0237
pg/mL
J
RANTES
p < 0.0001
pg/mL
Uninfected
DTV
POWV